applied sciences

MDPI

Article

Closed Form Solutions for Thermal Buckling of Functionally Graded Rectangular Thin Plates

Yufeng Xing * and Zekun Wang

Institute of Solid Mechanics, Beihang University, Beijing 100191, China; zkwang@buaa.edu.cn
* Correspondence: xingyf@buaa.edu.cn

Received: 31 October 2017; Accepted: 30 November 2017; Published: 3 December 2017

Abstract: This work concerns the critical buckling temperature of functionally graded rectangular thin plates; the properties of functionally graded material vary continuously in accordance with the power law of thickness z. Closed form solutions for the critical thermal parameter are obtained for the plate with the following boundary condition combinations: simply supported, clamped and guided edges, under uniform, linear and nonlinear temperature fields via the separation-of-variable method. Furthermore, a new method is proposed to determine the critical buckling temperature from the critical thermal parameter. The present results coincide well with those in the literature, verifying the correctness of the present method. The influences of the length–thickness ratio, length–width ratio, power law index and initial temperature on critical buckling temperature are investigated.

Keywords: functionally graded materials; thermal buckling; rectangular thin plates; critical temperature; closed form solution

1. Introduction

Designable Functionally Graded Materials (FGMs) are increasingly widely used in the aerospace, nuclear, and ship industries and other various industry departments, especially in thermal environments with ultra-high temperatures and a large temperature gradient. FGMs were proposed as thermal barrier materials by Japanese scientist Koizumi [1,2] to solve many problems in the new generation of aerospace airplane thermal protection systems. The volume content of each material in FGMs is continuously distributed in the spatial position on the macroscopic scale, and the physical properties change smoothly, so that the stress concentration of FGMs can be better avoided or reduced.

Since FGMs usually work in extremely high temperature environments, in order to ensure structural stability, the critical buckling temperature of FGM structures is very important in theory and application. Many researchers have studied the thermal buckling of FGM plates based on different theories in the past two decades.

Javaheri and Eslami [3] developed closed form solutions for the thermal buckling of simply supported FGM thin plates based on the Classical thin Plate Theory (CPT). Shariat and Eslami [4] obtained closed form solutions for the thermal buckling of simply supported imperfect FGM thin plates. Kiani et al. [5] investigated the critical buckling temperature of fully clamped FGM thin plates resting on elastic foundations; they used the Bubnov–Galerkin Solution (BGS), Power Series Solution (PSS) and Semi-Levy Solution (SLS) respectively to represent the lateral displacement which cannot be obtained by the Navier solution, and compared the solutions using these different approaches. Chu et al. [6] studied the critical buckling load and buckling model of FGM thin plate with in-plane material inhomogeneity by using radial basis function, but the thermal environment was not taken into account in their work.

Shear deformation plays a more prominent role for thick plates, so shear deformation theories are more accurate than CPT in this case. Wu [7] and Bouazza et al. [8] obtained a closed form solution for

thermal buckling of simply supported FGM thick plates based on the first-order shear deformation theory (FSDT), and compared the results with those of CPT. Shariat and Eslami [9] developed closed form solutions for thermal buckling of imperfect simply supported FGM thick plates based on FSDT. Lee et al. [10] obtained a finite element solution for the critical buckling temperature based on neutral surface and FSDT. Park and Kim [11] presented thermal postbuckling and vibration analyses based on FSDT by using the nonlinear finite element method. Cong and Duc [12] studied the thermal stability of eccentrically stiffened sigmoid FGM thick plate with metal–ceramic–metal layers by the Galerkin method based on FSDT.

There are also some researches based on high-order shear deformation theories. Javaheri and Eslami [13] developed closed form solutions for thermal buckling of simply supported FGM thick plates based on the third-order shear deformation theory (TSDT). Najafizadeh and Heydari [14] investigated the critical buckling temperature of clamped FGM circular thick plates based on TSDT, and compared it with results based on CPT and FSDT. Matsunaga [15] investigated the critical buckling temperature of simply supported FGM thick plates based on the 2D higher-order deformation theory that he developed, and compared the results with CPT and other lower-order shear deformation theories such as FSDT and TSDT. Zenkour and Mashat [16] studied thermal buckling of simply supported FGM thick plates based on sinusoidal shear deformation plate theory (SPT) and obtained closed form solutions.

Some researchers have used three-dimensional linear elasticity theory to analyze the thermal buckling of FGM plates. Na and Kim [17] studied the critical buckling temperature of FGM plates with various boundary conditions under uniform, linear and sinusoidal temperature fields by establishing the finite element model via three-dimensional linear elasticity theory. Subsequently, Na and Kim [18] improved their previous work and studied the thermal buckling of FGM composite structures. Malekzadeh [19] investigated the thermal buckling of FGM arbitrary straight-sided quadrilateral plates via the differential quadrature method (DQM) based on three-dimensional linear elasticity theory. Asemi et al. [20] investigated buckling of functionally graded plates under biaxial compression, shear, tension-compression, and shear-compression load conditions by establishing a full compatible three-dimensional elasticity element, but they didn't consider the thermal environment in their work. A review paper of various modeling techniques and solution methods in thermal analysis of FGM plates was also published [21].

From the above reviews, it can be seen that closed form solutions for thermal buckling of FGM plates are only available for a few boundary conditions such as fully simply supported parallel edges. Furthermore, there is currently no literature on the closed form solution for the critical buckling temperature of FGM thin plates for other boundary conditions. Furthermore, closed form solutions can play a reference role to study the convergence and precision of various numerical methods and serve the purpose of parametric designs of structures.

In the context of closed form solutions for the critical thermal parameter of simply supported FGM rectangular thin plates, guide and clamp boundary conditions are obtained via the separation-of-variable method. A novel method is presented to determine the critical buckling temperature from the critical thermal parameter. It is assumed that the FGM properties follow the power law distribution in the thickness direction. Two types of FGM thin plates and uniform, linear and nonlinear temperature fields are taken into account. The influences of the length–thickness ratio, length–width ratio, power law index and initial temperature on the critical buckling temperature are investigated in detail.

2. Governing Equation of Thermal Buckling

In this work, the FGM rectangular plate of length a, width b and thickness h is investigated as shown in Figure 1.

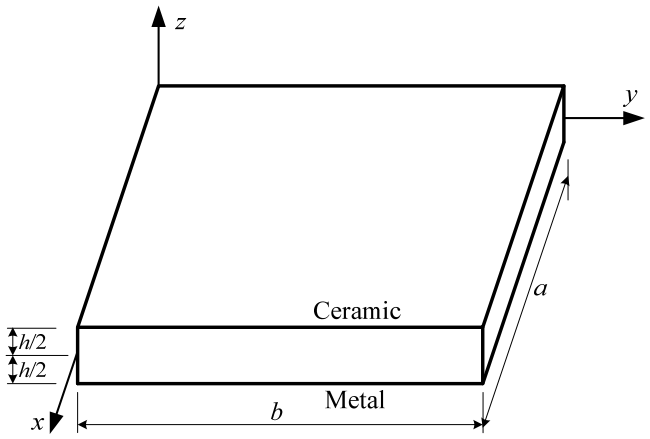

Figure 1. Functionally Graded Material (FGM) thin plate and Cartesian coordinates.

CPT is used with the following displacement fields

$$\begin{aligned} u &= u_0 - z\frac{\partial w}{\partial x} \\ v &= v_0 - z\frac{\partial w}{\partial y} \\ w &= w_0 \end{aligned} \tag{1}$$

where u_0 and v_0 are the in-plane displacements on the midplane of the plate along the x and y direction, respectively; w is the midplane deflection. The strains associated with the displacement fields in Equation (1) are

$$\begin{bmatrix} \varepsilon_{xx} \\ \varepsilon_{yy} \\ \varepsilon_{xy} \end{bmatrix} = \begin{bmatrix} \dfrac{\partial u_0}{\partial x} - z\dfrac{\partial^2 w}{\partial x^2} \\ \dfrac{\partial v_0}{\partial y} - z\dfrac{\partial^2 w}{\partial y^2} \\ \dfrac{\partial u_0}{\partial y} + \dfrac{\partial v_0}{\partial x} - 2z\dfrac{\partial^2 w}{\partial x \partial y} \end{bmatrix} \tag{2}$$

The constitutive relation for the FGM plate subjected to thermo-mechanical loadings is

$$\begin{bmatrix} \sigma_{xx} \\ \sigma_{yy} \\ \sigma_{xy} \end{bmatrix} = \frac{E}{1-\nu^2}\begin{bmatrix} 1 & \nu & 0 \\ \nu & 1 & 0 \\ 0 & 0 & \frac{1-\nu}{2} \end{bmatrix}\left(\begin{bmatrix} \varepsilon_{xx} \\ \varepsilon_{yy} \\ \varepsilon_{xy} \end{bmatrix} - \Delta T\begin{bmatrix} \alpha \\ \alpha \\ 0 \end{bmatrix}\right) \tag{3}$$

The stress resultants can be written as

$$\begin{aligned} \left(N_{xx}, N_{yy}, N_{xy}\right) &= \int_{-h/2}^{h/2}\left(\sigma_{xx}, \sigma_{yy}, \sigma_{xy}\right)\mathrm{d}z \\ \left(M_{xx}, M_{yy}, M_{xy}\right) &= \int_{-h/2}^{h/2} z\left(\sigma_{xx}, \sigma_{yy}, \sigma_{xy}\right)\mathrm{d}z \end{aligned} \tag{4}$$

Substituting Equations (1)–(3) into Equation (4) yields

$$\begin{aligned}
\begin{bmatrix} N_{xx} \\ M_{xx} \end{bmatrix} &= \begin{bmatrix} \int_{-h/2}^{h/2} \left\{ \frac{E}{1-\nu^2} \left[\frac{\partial u_0}{\partial x} - z\frac{\partial^2 w}{\partial x^2} + \nu\left(\frac{\partial v_0}{\partial y} - z\frac{\partial^2 w}{\partial y^2} \right) \right] \right\} \mathrm{d}z - N_T \\ \int_{-h/2}^{h/2} \left\{ \frac{Ez}{1-\nu^2} \left[\frac{\partial u_0}{\partial x} - z\frac{\partial^2 w}{\partial x^2} + \nu\left(\frac{\partial v_0}{\partial y} - z\frac{\partial^2 w}{\partial y^2} \right) \right] \right\} \mathrm{d}z - M_T \end{bmatrix} \\
\begin{bmatrix} N_{yy} \\ M_{yy} \end{bmatrix} &= \begin{bmatrix} \int_{-h/2}^{h/2} \left\{ \frac{E}{1-\nu^2} \left[\frac{\partial v_0}{\partial y} - z\frac{\partial^2 w}{\partial y^2} + \nu\left(\frac{\partial u_0}{\partial x} - z\frac{\partial^2 w}{\partial x^2} \right) \right] \right\} \mathrm{d}z - N_T \\ \int_{-h/2}^{h/2} \left\{ \frac{Ez}{1-\nu^2} \left[\frac{\partial v_0}{\partial y} - z\frac{\partial^2 w}{\partial y^2} + \nu\left(\frac{\partial u_0}{\partial x} - z\frac{\partial^2 w}{\partial x^2} \right) \right] \right\} \mathrm{d}z - M_T \end{bmatrix} \\
\begin{bmatrix} N_{xy} \\ M_{xy} \end{bmatrix} &= \begin{bmatrix} \int_{-h/2}^{h/2} \left[\frac{E}{2(1+\nu)} \left(\frac{\partial u_0}{\partial y} + \frac{\partial v_0}{\partial x} - 2z\frac{\partial^2 w}{\partial x \partial y} \right) \right] \mathrm{d}z \\ \int_{-h/2}^{h/2} \left[\frac{Ez}{2(1+\nu)} \left(\frac{\partial u_0}{\partial y} + \frac{\partial v_0}{\partial x} - 2z\frac{\partial^2 w}{\partial x \partial y} \right) \right] \mathrm{d}z \end{bmatrix}
\end{aligned} \tag{5}$$

where

$$\begin{aligned}
N_T &= \int_{-h/2}^{h/2} \frac{E\alpha\Delta T}{1-\nu} \mathrm{d}z \\
M_T &= \int_{-h/2}^{h/2} \frac{E\alpha\Delta T z}{1-\nu} \mathrm{d}z
\end{aligned} \tag{6}$$

From Equation (5), it can be seen that the in-plane loading and bending of the plate couple together because there is in-plane stretching in the geometrical midplane due to the materials' asymmetry with respect to the midplane. However, the coupling can be eliminated by choosing the neutral surface instead of the geometrical midplane as a reference surface in which there are no in-plane displacements [22] (p. 1091).

The in-plane displacements of the midplane can be expressed as

$$u_0 = z_0 \frac{\partial w}{\partial x}, \qquad v_0 = z_0 \frac{\partial w}{\partial y} \tag{7}$$

where z_0 is the distance between the geometrical midplane and the neutral surface. Substituting Equation (7) into Equation (5) yields

$$\begin{aligned}
\begin{bmatrix} N_{xx} \\ M_{xx} \end{bmatrix} &= \begin{bmatrix} \int_{-h/2}^{h/2} \left[\frac{E(z_0 - z)}{1-\nu^2} \left(\frac{\partial^2 w}{\partial x^2} + \nu\frac{\partial^2 w}{\partial y^2} \right) \right] \mathrm{d}z - N_T \\ \int_{-h/2}^{h/2} \left[\frac{Ez(z_0 - z)}{1-\nu^2} \left(\frac{\partial^2 w}{\partial x^2} + \nu\frac{\partial^2 w}{\partial y^2} \right) \right] \mathrm{d}z - M_T \end{bmatrix} \\
\begin{bmatrix} N_{yy} \\ M_{yy} \end{bmatrix} &= \begin{bmatrix} \int_{-h/2}^{h/2} \left[\frac{E(z_0 - z)}{1-\nu^2} \left(\frac{\partial^2 w}{\partial y^2} + \nu\frac{\partial^2 w}{\partial x^2} \right) \right] \mathrm{d}z - N_T \\ \int_{-h/2}^{h/2} \left[\frac{Ez(z_0 - z)}{1-\nu^2} \left(\frac{\partial^2 w}{\partial y^2} + \nu\frac{\partial^2 w}{\partial x^2} \right) \right] \mathrm{d}z - M_T \end{bmatrix} \\
\begin{bmatrix} N_{xy} \\ M_{xy} \end{bmatrix} &= \begin{bmatrix} \int_{-h/2}^{h/2} \left(\frac{E(z_0 - z)}{1+\nu} \frac{\partial^2 w}{\partial x \partial y} \right) \mathrm{d}z \\ \int_{-h/2}^{h/2} \left(\frac{Ez(z_0 - z)}{1+\nu} \frac{\partial^2 w}{\partial x \partial y} \right) \mathrm{d}z \end{bmatrix}
\end{aligned} \tag{8}$$

From Equation (8), it can be seen that the in-plane loading and bending of the plate have been decoupled.

The total potential energy of a plate in a thermal environment is [23,24]

$$U = \frac{1}{2} \int_V \{ \sigma_{xx}(\varepsilon_{xx} - \alpha\Delta T) + \sigma_{yy}(\varepsilon_{yy} - \alpha\Delta T) + \sigma_{xy}\varepsilon_{xy} \} \mathrm{d}V \tag{9}$$

Using Equation (8) and employing the Euler equations to minimize the total potential energy function yields the equilibrium equations of an FGM plate

$$\begin{aligned}
&\frac{\partial N_{xx}}{\partial x}+\frac{\partial N_{xy}}{\partial y}=0\\
&\frac{\partial N_{xy}}{\partial x}+\frac{\partial N_{yy}}{\partial y}=0\\
&\frac{\partial^2 M_{xx}}{\partial x^2}+\frac{\partial^2 M_{yy}}{\partial y^2}+2\frac{\partial^2 M_{xy}}{\partial x\partial y}+N_{xx}\frac{\partial^2 w}{\partial x^2}+2N_{xy}\frac{\partial^2 w}{\partial x\partial y}+N_{yy}\frac{\partial^2 w}{\partial y^2}=0
\end{aligned} \tag{10}$$

Substituting Equation (8) into Equation (10) determines the distance z_0 and yields the thermal buckling that governs the equation of an FGM thin rectangular plate as

$$z_0=\frac{B_{11}+G_1}{A_{11}+G_0} \tag{11}$$

$$\left(D_{11}+G_2-\frac{(B_{11}+G_1)^2}{A_{11}+G_0}\right)\left(\frac{\partial^4 w}{\partial x^4}+2\frac{\partial^4 w}{\partial x^2\partial y^2}+\frac{\partial^4 w}{\partial y^4}\right)-G_0\left(\frac{\partial^2 w}{\partial x^2}+\frac{\partial^2 w}{\partial y^2}\right)=0 \tag{12}$$

or

$$\left(\frac{\partial^4 w}{\partial x^4}+2\frac{\partial^4 w}{\partial x^2\partial y^2}+\frac{\partial^4 w}{\partial y^4}\right)+\hat{G}_0\left(\frac{\partial^2 w}{\partial x^2}+\frac{\partial^2 w}{\partial y^2}\right)=0 \tag{13}$$

where

$$\begin{aligned}
l\hat{G}_0&=\frac{-G_0}{D_{11}+G_2-\dfrac{(B_{11}+G_1)^2}{A_{11}+G_0}}\\
G_i&=-\int_{-\frac{h}{2}}^{\frac{h}{2}} z^i\frac{\alpha E}{1-\nu}(T-T_0)\mathrm{d}z(i=0,1,2)\\
(A_{ij},B_{ij},D_{ij})&=\int_{-\frac{h}{2}}^{\frac{h}{2}} Q_{ij}\left(1,z,z^2\right)\mathrm{d}z(i,j=1,2,6)
\end{aligned} \tag{14}$$

$$\begin{aligned}
Q_{11}&=Q_{22}=\frac{E}{1-\nu^2}\\
Q_{12}&=Q_{21}=\frac{\nu E}{1-\nu^2}\\
Q_{66}&=\frac{E}{2(1+\nu)}
\end{aligned} \tag{15}$$

where the Young's modulus E, mass density ρ, Poisson's ratio ν, thermal conductivity k and thermal expansion coefficient α of FGM vary continuously with thickness z as

$$P=(P_\mathrm{t}-P_\mathrm{b})\left(\frac{1}{2}+\frac{z}{h}\right)^n+P_\mathrm{b} \tag{16}$$

where P stands for E, ν, α, k and ρ, respectively, and the subscripts t and b stand for the top and bottom surfaces of the plate, respectively. n is the power law index indicating the material variation profile through the thickness, and n = 0 represents a homogeneous plate. The material properties are also related to temperature by the following relation:

$$\frac{P}{P_0}=P_{-1}T(z)^{-1}+1+P_1T(z)+P_2T(z)^2+P_3T(z)^3 \tag{17}$$

where P_{-1}, P_0, P_1, P_2 and P_3 are the constants only related to the material, and T is the temperature function.

The temperature distribution of the uniform temperature field is

$$T(z) = T_0 + \Delta T \tag{18}$$

which is independent of thickness z.

The temperature distribution of the linear temperature field is

$$T(z) = T_0 + \Delta T\left(\frac{1}{2} + \frac{z}{h}\right) \tag{19}$$

The temperature changes from T_0 to $T_0 + \Delta T$ linearly as the thickness varies from $-h/2$ to $h/2$.

The nonlinear temperature field is from the one-dimensional thermal conduction equation:

$$-\frac{\mathrm{d}}{\mathrm{d}z}\left[k(z)\frac{\mathrm{d}T}{\mathrm{d}z}\right] = 0 \tag{20}$$

Note that the thermal conductivity of materials $k(z)$ is independent of temperature T, so the analytical solution of Equation (20) can be obtained as

$$T(z) = T_0 + \Delta T\frac{\int_{-\frac{h}{2}}^{z}\frac{1}{k(z)}\mathrm{d}z}{\int_{-\frac{h}{2}}^{\frac{h}{2}}\frac{1}{k(z)}\mathrm{d}z} \tag{21}$$

Substituting Equation (16) into Equation (21) yields the nonlinear temperature field as

$$T(z) = T_0 + \Delta T \cdot f(z) \tag{22}$$

where

$$\begin{aligned} f(z) &= \frac{\sum_{j=0}^{5}\frac{(-1)^j\Delta k^j}{(j\times n+1)k_{\mathrm{b}}^j}\left(\frac{z}{h}+\frac{1}{2}\right)^{j\times n+1}}{\sum_{j=0}^{5}\frac{(-1)^j\Delta k^j}{(j\times n+1)k_{\mathrm{b}}^j}} \\ \Delta k &= k_{\mathrm{t}} - k_{\mathrm{b}} \end{aligned} \tag{23}$$

k_{t} and k_{b} are thermal conductivities at the top and bottom surfaces of the plate, respectively.

3. Closed Form Solutions of Thermal Buckling

After establishing the thermal buckling governing equation, the material model and temperature fields, the buckling solutions including thermal buckling mode function and critical buckling temperature are obtained below in separation-of-variable form.

Assuming that Equation (12) has the following separation-of-variable solution:

$$w(x,y) = \phi(x)\psi(y) \tag{24}$$

where w is the buckling mode function, and

$$\phi(x) = A\mathrm{e}^{\vartheta x}, \psi(y) = B\mathrm{e}^{\eta y} \tag{25}$$

where ϑ and η are unknown spatial eigenvalues. Substituting Equations (24) and (25) into Equation (12) yields the relation of ϑ, η and $\hat{G}_0$ as

$$\left(\hat{G}_0 + \vartheta^2 + \eta^2\right)\left(\vartheta^2 + \eta^2\right) = 0 \tag{26}$$

From Equation (26), we have the following relations

$$\begin{aligned} \vartheta_{1,2} &= \pm\alpha_2 = \pm\sqrt{-\eta^2} \\ \vartheta_{3,4} &= \pm\mathrm{i}\alpha_1 = \pm\mathrm{i}\sqrt{\eta^2 + \hat{G}_0} \\ \eta_{1,2} &= \pm\beta_2 = \pm\sqrt{-\vartheta^2} \\ \eta_{3,4} &= \pm\mathrm{i}\beta_1 = \pm\mathrm{i}\sqrt{\vartheta^2 + \hat{G}_0} \end{aligned} \tag{27}$$

Therefore, the functions $\phi(x)$ and $\psi(y)$ have the following closed forms:

$$\begin{aligned} \phi(x) &= A_2\cos\alpha_1 x + B_2\sin\alpha_1 x + C_2\cosh\alpha_2 x + D_2\sinh\alpha_2 x \\ \psi(y) &= A_1\cos\beta_1 y + B_1\sin\beta_1 y + C_1\cosh\beta_2 y + D_1\sinh\beta_2 y \end{aligned} \tag{28}$$

where the five unknown variables α_1, α_2, β_1, β_2 and $\hat{G}_0$ are involved; then, four equations are needed for a unique solution. From Equation (27), one can obtain three relations of these five variables:

$$\begin{aligned} \alpha_1^2 + \alpha_2^2 &= \hat{G}_0 \\ \beta_1^2 + \beta_2^2 &= \hat{G}_0 \end{aligned} \tag{29}$$

$$\alpha_1{}^2 + \beta_1{}^2 = \vartheta^2 + \eta^2 + 2\hat{G}_0 \tag{30}$$

Substituting $\vartheta = \pm\mathrm{i}\alpha_1$, $\eta = \pm\mathrm{i}\beta_1$ into Equation (30) yields

$$\alpha_1{}^2 + \beta_1{}^2 = \hat{G}_0 \tag{31}$$

Another two transcendental eigenvalue equations can be derived by using the two pairs of boundary conditions of four edges. The boundary conditions used in this study are presented in Table 1 where n denotes the outer normal direction of the edge.

Table 1. Boundary conditions of a rectangular plate.

Simple Support (S)	$w = 0$	$M_n = 0$
Guide (G)	$\dfrac{\partial w}{\partial n} = 0$	$Q_n = 0$
Clamp (C)	$w = 0$	$\dfrac{\partial w}{\partial n} = 0$

The buckling mode functions have the separation-of-variable form as shown in Equation (24); then, the two transcendental eigenvalue equations can be derived separately by considering the boundary conditions with respect to x and y, respectively. Substituting the two eigenfunctions in Equation (28) into the boundary conditions given in Table 1 yields the transcendental eigenvalue equations which are shown in Table 2 [25–27].

By using Equation (29), Equation (31) and two transcendental eigenvalue equations corresponding to specific boundary conditions of a rectangular plate, we can solve the five variables α_1, α_2, β_1, β_2 and $\hat{G}_0$. For clarity of discussion, the solved $\hat{G}_0$ from eigenvalue equations is denoted by $\hat{G}_{0\mathrm{cr}}$.

Table 2. Eigenvalue equations for various boundary conditions.

B.C.	Eigenvalue Equations for y = 0 and b	Eigenvalue Equations for x = 0 and a
S-S	$\sin\beta_1 b = 0$	$\sin\alpha_1 a = 0$
G-G	$\sin\beta_1 b = 0$	$\sin\alpha_1 a = 0$
C-C	$\frac{1-\cos\beta_1 b\cosh\beta_2 b}{\sin\beta_1 b\sinh\beta_2 b} = \frac{\beta_1^2-\beta_2^2}{2\beta_1\beta_2}$	$\frac{1-\cos\alpha_1 a\cosh\alpha_2 a}{\sin\alpha_1 a\sinh\alpha_2 a} = \frac{\alpha_1^2-\alpha_2^2}{2\alpha_1\alpha_2}$
S-G	$\cos\beta_1 b = 0$	$\cos\alpha_1 a = 0$
S-C	$\beta_2\tan\beta_1 b = \beta_1\tanh\beta_2 b$	$\alpha_2\tan\alpha_1 a = \alpha_1\tanh\alpha_2 a$
G-C	$\beta_1\tan\beta_1 b = -\beta_2\tanh\beta_2 b$	$\alpha_1\tan\alpha_1 a = -\alpha_2\tanh\alpha_2 a$

Note that $\hat{G}_{0\mathrm{cr}}$ is a critical thermal buckling parameter in which the critical temperature is involved, but in general it is hard or impossible to directly extract the explicit form of the critical buckling temperature T_{cr} from $\hat{G}_{0\mathrm{cr}}$. In the present study, a novel method of determining T_{cr} is proposed. To achieve this aim, an algebraic equation for the critical buckling temperature is given as

$$\hat{G}_0(T) = \hat{G}_{0\mathrm{cr}} \tag{32}$$

where $\hat{G}_0(T)$ is given in Equation (14); it is a function of temperature, material properties and plate thickness, and T_{cr} can be solved numerically from Equation (31). For three simple cases, analytical solutions can be found; the details are given in the following.

3.1. Case 1 Temperature-Independent Homogeneous Thin Plates

For homogeneous isotropic plates, the material properties are independent of geometry and temperature. According to Equation (14), $\hat{G}_0$ can be written as

$$\hat{G}_0 = \frac{-G_0}{D_{11}+G_2-\frac{(B_{11}+G_1)^2}{A_{11}+G_0}} = \frac{(1+\nu)\alpha\left(\int_{-h/2}^{h/2} T\mathrm{d}z - T_0 h\right)}{\frac{h^3}{12}-(1+\nu)\alpha\left(\int_{-h/2}^{h/2} Tz^2\mathrm{d}z - \frac{T_0 h^3}{12}\right)} \tag{33}$$

then, the analytical critical temperature can be solved from Equation (31). For a uniform temperature field, it is

$$\Delta T_{\mathrm{cr,uni}} = \frac{\hat{G}_{0\mathrm{cr}}h^2}{\alpha(1+\nu)\left(\hat{G}_{0\mathrm{cr}}h^2+12\right)} \tag{34}$$

where $\Delta T_{\mathrm{cr}} = T_{\mathrm{cr}} - T_0$; for a linear temperature field, it is

$$\Delta T_{\mathrm{cr,line}} = \frac{2\hat{G}_{0\mathrm{cr}}h^2}{\alpha(1+\nu)\left(\hat{G}_{0\mathrm{cr}}h^2+12\right)} \tag{35}$$

It can be seen that, for the temperature-independent homogeneous isotropic thin plates, we have

$$\Delta T_{\mathrm{cr,line}} = 2\Delta T_{\mathrm{cr,uni}} \tag{36}$$

The nonlinear temperature field does not exist for homogeneous isotropic plates since the thermal conductivities at the top and bottom surfaces are the same. Substituting $k_{\mathrm{t}} = k_{\mathrm{b}}$ into Equation (23), we can find that the temperature distribution of the nonlinear temperature field reduces to the linear temperature field.

3.2. Case 2 Temperature-Independent FGM Thin Plates

In this case, the FGM thin plates have temperature-independent material properties which vary with the thickness following the power law in Equation (16). For a uniform temperature field, $\hat{G}_0$ follows from Equation (14) that

$$\hat{G}_0 = \frac{\Delta T \cdot \int_{-h/2}^{h/2} \frac{\alpha E}{1-\nu} \mathrm{d}z}{\int_{-h/2}^{h/2} \frac{Ez^2}{1-\nu^2} \mathrm{d}z - \Delta T \cdot \int_{-h/2}^{h/2} \frac{\alpha E z^2}{1-\nu} \mathrm{d}z - \frac{\left(\int_{-h/2}^{h/2} \frac{Ez}{1-\nu^2} \mathrm{d}z - \Delta T \cdot \int_{-h/2}^{h/2} \frac{\alpha E z}{1-\nu} \mathrm{d}z \right)^2}{\int_{-h/2}^{h/2} \frac{E}{1-\nu^2} \mathrm{d}z - \Delta T \cdot \int_{-h/2}^{h/2} \frac{\alpha E}{1-\nu} \mathrm{d}z}} \tag{37}$$

Then, the critical buckling temperature is

$$\Delta T_{\mathrm{cr}} = \frac{\hat{G}_{0\mathrm{cr}} J_0 J_1 + \hat{G}_{0\mathrm{cr}} J_2 J_5 - 2\hat{G}_{0\mathrm{cr}} J_3 J_4 + J_0 J_5 - \sqrt{\Theta}}{2\left(\hat{G}_{0\mathrm{cr}} J_0 J_2 - \hat{G}_{0\mathrm{cr}} {J_4}^2 + {J_0}^2\right)} \tag{38}$$

where

$$\begin{aligned} \Theta = \; & \hat{G}_{0\mathrm{cr}}^2 J_0^2 J_0^1 - 2\hat{G}_{0\mathrm{cr}}^2 J_0 J_1 J_2 J_5 - 4\hat{G}_{0\mathrm{cr}}^2 J_0 J_1 J_3 J_4 + 4\hat{G}_{0\mathrm{cr}}^2 J_0 J_2 J_3^2 \\ & + 4\hat{G}_{0\mathrm{cr}}^2 J_1 J_4^2 J_5 + \hat{G}_{0\mathrm{cr}}^2 J_2^2 J_5^2 - 4\hat{G}_{0\mathrm{cr}}^2 J_2 J_3 J_4 J_5 - 2\hat{G}_{0\mathrm{cr}} J_0^2 J_1 J_5 \\ & + 4\hat{G}_{0\mathrm{cr}} J_0^2 J_2^3 + 2\hat{G}_{0\mathrm{cr}} J_0 J_2 J_5^2 - 4\hat{G}_{0\mathrm{cr}} J_0 J_3 J_4 J_5 + J_0^2 J_2^5 \end{aligned} \tag{39}$$

The critical buckling temperature for linear and nonlinear temperature fields can be obtained similarly. Table 3 presents the integrals J_0 ~J_5 which can be calculated numerically, and $f(z)$ is given in Equation (23). It is noteworthy that the critical buckling temperature is irrelevant to the initial temperature for temperature-independent materials.

Table 3. The integrals in Equation (38).

Integral	Uniform Temperature Field	Linear Temperature Field	Nonlinear Temperature Field
J_0	$\int_{-h/2}^{h/2} \frac{\alpha E}{1-\nu} \mathrm{d}z$	$\int_{-h/2}^{h/2} \frac{\alpha E}{1-\nu} \left(\frac{1}{2} + \frac{z}{h}\right) \mathrm{d}z$	$\int_{-h/2}^{h/2} \frac{\alpha E}{1-\nu} f(z) \mathrm{d}z$
J_1	$\int_{-h/2}^{h/2} \frac{Ez^2}{1-\nu^2} \mathrm{d}z$	$\int_{-h/2}^{h/2} \frac{Ez^2}{1-\nu^2} \left(\frac{1}{2} + \frac{z}{h}\right) \mathrm{d}z$	$\int_{-h/2}^{h/2} \frac{Ez^2}{1-\nu^2} f(z) \mathrm{d}z$
J_2	$\int_{-h/2}^{h/2} \frac{\alpha E z^2}{1-\nu} \mathrm{d}z$	$\int_{-h/2}^{h/2} \frac{\alpha E z^2}{1-\nu} \left(\frac{1}{2} + \frac{z}{h}\right) \mathrm{d}z$	$\int_{-h/2}^{h/2} \frac{\alpha E z^2}{1-\nu} f(z) \mathrm{d}z$
J_3	$\int_{-h/2}^{h/2} \frac{Ez}{1-\nu^2} \mathrm{d}z$	$\int_{-h/2}^{h/2} \frac{Ez}{1-\nu^2} \left(\frac{1}{2} + \frac{z}{h}\right) \mathrm{d}z$	$\int_{-h/2}^{h/2} \frac{Ez}{1-\nu^2} f(z) \mathrm{d}z$
J_4	$\int_{-h/2}^{h/2} \frac{\alpha E z}{1-\nu} \mathrm{d}z$	$\int_{-h/2}^{h/2} \frac{\alpha E z}{1-\nu} \left(\frac{1}{2} + \frac{z}{h}\right) \mathrm{d}z$	$\int_{-h/2}^{h/2} \frac{\alpha E z}{1-\nu} f(z) \mathrm{d}z$
J_5	$\int_{-h/2}^{h/2} \frac{E}{1-\nu^2} \mathrm{d}z$	$\int_{-h/2}^{h/2} \frac{E}{1-\nu^2} \left(\frac{1}{2} + \frac{z}{h}\right) \mathrm{d}z$	$\int_{-h/2}^{h/2} \frac{E}{1-\nu^2} f(z) \mathrm{d}z$

3.3. Case 3 Temperature-Dependent Homogeneous Plates for a Uniform Temperature Field

Referring to Equations (14) and (17), in this case $\hat{G}_0$ can be written as

$$\hat{G}_0 = \frac{12\alpha_0 \left(1 + \nu_0 \Upsilon_1\right) \Upsilon_2 \Delta T}{h^2 \left[1 - \alpha_0 \left(1 + \nu_0 \Upsilon_1\right) \Upsilon_2 \Delta T\right]} \tag{40}$$

where

$$\begin{aligned}\Upsilon_1 &= \frac{\nu_{-1}}{T_0+\Delta T}+1+\nu_1(T_0+\Delta T)+\nu_2(T_0+\Delta T)^2+\nu_3(T_0+\Delta T)^3\\ \Upsilon_2 &= \frac{\alpha_{-1}}{T_0+\Delta T}+1+\alpha_1(T_0+\Delta T)+\alpha_2(T_0+\Delta T)^2+\alpha_3(T_0+\Delta T)^3\end{aligned} \tag{41}$$

It can be proved that ΔT_{cr} is one of the roots of the following ninth-order algebraic equation

$$A_9x^9+A_8x^8+A_7x^7+A_6x^6+A_5x^5+A_4x^4+A_3x^3+A_2x^2+A_1x+A_0=0 \tag{42}$$

where the coefficients are given in Appendix A. Equation (42) can be solved by the numerical methods to obtain the critical buckling temperature for a uniform temperature field. In general, the critical buckling temperature should be the smallest positive solution of the nine-order algebraic equation. It can be seen that the initial temperature T_0 affects the critical buckling temperature of temperature-dependent homogeneous plates under a uniform temperature field. The results provided later demonstrate the effect of T_0 for temperature-dependent FGM plates under all kinds of thermal environments.

3.4. Case 4 Other Situations

Except for the above three cases, it is difficult to obtain the explicit expression of the critical buckling temperature, and Equation (32) must be solved numerically for T_{cr}.

In this study, the secant method is used to solve

$$\hat{G}_0(T)-\hat{G}_{0\mathrm{cr}}=0 \tag{43}$$

because it is difficult to determine the derivative $\mathrm{d}\hat{G}_0/\mathrm{d}T$. Let $x = T$ and

$$g(x)=\hat{G}_0(T)-\hat{G}_{0\mathrm{cr}} \tag{44}$$

Given two initial values x_{-1} and x_0, the iterative scheme of the secant method is

$$x_{k+1}=x_k-\frac{g(x_k)(x_k-x_{k-1})}{g(x_k)-g(x_{k-1})},\quad (k=0,1,\cdots) \tag{45}$$

When x_k and x_{k-1} satisfy

$$\frac{|x_k-x_{k-1}|}{|x_k|}\le\eta \tag{46}$$

the iteration stops, where the relative tolerance $\eta > 0$.

4. Numerical Results and Discussion

Two types of FGM thin plates are considered in this section. Type-I FGM plate is temperature-dependent; it is made from stainless steel (SUS304) and Silicon nitride (Si_3N_4). The material properties are shown in Table 4. Type-II FGM plate is temperature-independent; it is made from aluminum as its bottom surface and aluminum oxide as its top surface. E_{t} = 70 GPa, $\alpha_{\mathrm{t}} = 23\times10^{-6}$/K, E_{b} = 380 GPa, $\alpha_{\mathrm{b}} = 7.4\times10^{-6}$/K, ν = 0.3. Plates with different boundary conditions investigated below are shown in Figure 2.

Firstly, the results of the present method are compared with those in the literature to validate the correctness of this method. Tables 5 and 6 compare the critical buckling temperature ΔT_{cr} of simply supported type-II FGM square plate based on different theories. Table 7 compares ΔT_{cr} of fully clamped type-II FGM rectangular plate. It can be seen that the present results coincide well with available results.

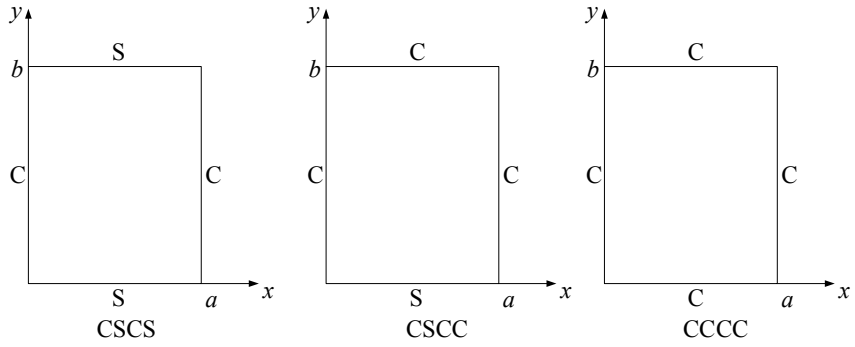

Figure 2. Plates with different boundary conditions.

Table 4. The material properties of type-I FGM plate.

Property	Material Type	P_{-1}	P_0	P_1	P_2	P_3
E	Si_3N_4	0	348.43×10^9	-3.070×10^{-4}	2.160×10^{-7}	-8.946×10^{-11}
	SUS304	0	201.04×10^9	3.079×10^{-4}	-6.534×10^{-7}	0
ν	Si_3N_4	0	0.2400	0	0	0
	SUS304	0	0.3262	-2.002×10^{-4}	3.797×10^{-7}	0
α	Si_3N_4	0	5.8723×10^{-6}	9.095×10^{-4}	0	0
	SUS304	0	12.330×10^{-6}	8.086×10^{-4}	0	0
ρ	Si_3N_4	0	2370	0	0	0
	SUS304	0	8166	0	0	0
k	Si_3N_4	0	9.19	0	0	0
	SUS304	0	12.04	0	0	0

Table 5. Critical buckling temperature ΔT_{cr} of SSSS type-II FGM square plate with different a/h under a uniform temperature field ($a/b = 1$).

n	Method	$a/h = 10$	$a/h = 20$	$a/h = 40$	$a/h = 60$	$a/h = 80$	$a/h = 100$
1	Present	782.016	197.813	49.600	22.056	12.409	7.943
	CPT [15]	794.377	198.594	49.648	22.066	12.412	7.943
	TSDT [15]	757.891	196.257	49.500	22.037	12.402	7.939
	HDT5 [15]	749.260	195.623	49.404	22.029	12.400	7.939
5	Present	713.894	180.841	45.361	20.173	11.350	7.265
	CPT [15]	726.571	181.642	45.410	20.182	11.352	7.265
	TSDT [15]	678.926	178.528	45.213	20.144	11.340	7.260
	HDT5 [15]	669.402	177.805	45.166	20.134	11.337	7.259
10	Present	733.217	185.863	46.629	20.737	11.667	7.468
	CPT [15]	746.927	186.731	46.682	20.747	11.670	7.469
	TSDT [15]	692.519	183.141	46.455	20.703	11.657	7.462
	HDT5 [15]	683.211	182.432	46.409	20.694	11.654	7.462

Table 6. Critical buckling temperature ΔT_{cr} of SSSS type-II FGM plate with different a/b under a uniform temperature field (a/h = 100).

n	Method	*a*/*b* = 1	*a*/*b* = 2	*a*/*b* = 3	*a*/*b* = 4	*a*/*b* = 5
1	Present	7.9426	19.8516	39.6876	67.4319	103.0568
	CPT [16]	7.9437	19.8594	39.7188	67.5220	103.2690
	FPT [16]	7.9400	19.8358	39.6248	67.2506	102.6355
	TSDT [16]	7.9400	19.8358	39.6248	67.2506	102.6356
	SSDT [16]	7.9400	19.8359	39.6249	67.2510	102.6365
2	Present	7.0415	17.5995	35.1851	59.7816	91.3644
	CPT [16]	7.0426	17.6065	35.2130	59.8621	91.5538
	FPT [16]	7.0392	17.5853	35.1285	59.6184	91.9850
	TSDT [16]	7.0390	17.5840	35.1234	59.6037	90.9508
	SSDT [16]	7.0390	17.5840	35.1233	59.6034	90.9501
5	Present	7.2645	18.1563	36.2964	61.6659	94.2363
	CPT [16]	7.2657	18.1642	36.3285	61.7585	94.4542
	FPT [16]	7.2615	18.1380	36.2236	61.4559	93.7481
	TSDT [16]	7.2606	18.1327	36.2025	61.3951	93.6069
	SSDT [16]	7.2606	18.1324	36.2014	61.3921	93.5999
10	Present	7.4679	18.6645	37.3115	63.3884	96.8646
	CPT [16]	7.4692	18.6731	37.3463	63.4888	97.1005
	FPT [16]	7.4644	18.6427	37.2246	63.1378	96.2820
	TSDT [16]	7.4634	18.6366	37.2006	63.0687	96.1213
	SSDT [16]	7.4634	18.6365	37.2001	63.0673	96.1183

Table 7. Critical buckling temperature ΔT_{cr} of CCCC type-II FGM rectangular plate under a uniform temperature field (a/h = 100, a/b = 2).

Method	*n* = 0	*n* = 0.5	*n* = 1	*n* = 2	*n* = 5	*n* = 10
Present	32.355	18.332	15.032	13.326	13.748	14.133
Kiani [5]	33.628	19.053	15.623	13.850	14.289	14.690

Tables 8 and 9 show ΔT_{cr} of type-I FGM thin plate under a uniform temperature field with different boundary conditions. The results indicate that fully clamped (CCCC) plates have the largest ΔT_{cr}, and ΔT_{cr} decreases as the power law index n increases. Tables 10 and 11 give ΔT_{cr} of Type-I FGM thin plate under different temperature fields. Due to the small difference between the temperature distribution of the linear temperature field and nonlinear temperature field, ΔT_{cr} under these two temperature fields is close. Furthermore, ΔT_{cr} under a uniform temperature field is obviously lower than that under the other two temperature fields, so a uniform temperature field affects ΔT_{cr} more significantly than the other two. Table 12 presents ΔT_{cr} of Type-I FGM thin plate with different initial temperatures T_0.

Table 8. Critical buckling temperature ΔT_{cr} of type-I FGM rectangular thin plate with different a/h and various B.C. under a uniform temperature field ($a/b = 2$, $T_0 = 300$ K).

B.C.	*n*	*a*/*h* = 20	*a*/*h* = 30	*a*/*h* = 40	*a*/*h* = 50	*a*/*h* = 60	*a*/*h* = 70	*a*/*h* = 80
CSCS	1	583.7802	306.6174	186.0370	123.9484	88.1339	65.7278	50.8301
	2	547.3748	283.8704	171.2913	113.7826	80.7593	60.1576	46.4854
	5	517.0574	264.5071	158.8189	105.2290	74.5765	55.4993	42.8584
CSCC	1	783.2272	431.1364	267.9431	181.1536	130.0341	97.5959	75.8125
	2	742.2713	401.3746	247.6355	166.7565	119.4051	89.4729	69.4245
	5	713.3132	376.0498	230.3741	154.5835	110.4567	82.6559	64.0761
CCCC	1	1057.5407	640.8390	413.1423	285.7974	208.3541	158.0883	123.7707
	2	1013.9656	602.6029	384.3119	264.3487	192.0395	145.3645	113.6185
	5	1030.1122	571.4283	359.7632	246.1036	178.2185	134.6260	105.0764

Note: 'B.C.' stands for Boundary Condition.

Table 9. Critical buckling temperature ΔT_{cr} of type-I FGM rectangular thin plate with different a/b and various B.C. under a uniform temperature field ($a/h = 100$, $T_0 = 300$ K).

B.C.	*n*	*a*/*b* = 2	*a*/*b* = 3	*a*/*b* = 4	*a*/*b* = 5	*a*/*b* = 6	*a*/*b* = 7
CSCS	1	32.9286	57.7537	92.8929	136.4766	187.0319	243.2765
	2	30.0846	52.8369	85.1409	125.3608	172.2154	224.5874
	5	27.7157	48.7288	78.6384	115.9968	159.6822	208.7213
CSCC	1	49.3892	100.7232	168.6840	248.9947	338.3012	433.8633
	2	45.1642	92.3546	155.1861	229.9260	313.6459	403.9628
	5	41.6377	85.3292	143.7844	213.7327	292.6429	378.5233
CCCC	1	81.4595	176.7382	295.2208	428.0121	568.5417	711.2512
	2	74.6176	162.6580	273.1802	398.4099	532.6899	671.3248
	5	68.8856	150.7570	254.4250	373.2176	502.7141	640.2733

Table 10. Critical buckling temperature ΔT_{cr} of type-I FGM rectangular thin plate with different a/h and various B.C. ($a/b = 2$, $n = 2$, $T_0 = 300$ K).

B.C.	T.F.	*a*/*h* = 20	*a*/*h* = 30	*a*/*h* = 40	*a*/*h* = 50	*a*/*h* = 60	*a*/*h* = 70
CSCS	uniform	547.3748	283.8704	171.2913	113.7826	80.7593	60.1576
	linear	1133.6559	581.2390	352.4874	235.3624	167.7132	125.2884
	nonlinear	1182.5836	607.9852	369.1144	246.6213	175.8071	131.3707
CSCC	uniform	742.2713	401.3746	247.6355	166.7565	119.4051	89.4729
	linear	1594.4982	822.6864	507.5211	343.2718	246.8452	185.6015
	nonlinear	1655.7434	859.5887	531.0572	359.4812	258.6364	194.5373
CCCC	uniform	1013.9656	602.6029	384.3119	264.3487	192.0395	145.3645
	linear	2230.3048	1256.9658	787.2933	541.4994	394.6294	299.7612
	nonlinear	2275.4643	1310.1371	822.7439	566.5211	413.1558	313.9882

Note: 'T.F.' represents Temperature Field.

Table 11. Critical buckling temperature ΔT_{cr} of type-I FGM rectangular thin plate with different a/b and various B.C. ($a/h = 100$, $n = 2$, $T_0 = 300$ K).

B.C.	T.F.	$a/b = 2$	$a/b = 3$	$a/b = 4$	$a/b = 5$	$a/b = 6$	$a/b = 7$
CSCS	uniform	30.0846	52.8369	85.1409	125.3608	172.2154	224.5874
	linear	62.9589	110.1631	176.7119	258.9990	354.3651	460.7078
	nonlinear	66.0438	115.5227	185.2298	271.3522	371.0771	482.1803
CSCC	uniform	45.1642	92.3546	155.1861	229.9260	313.6459	403.9628
	linear	94.2791	191.5108	319.7465	471.5480	642.0001	828.0680
	nonlinear	98.8767	200.7238	334.8863	493.5001	671.3553	865.1898
CCCC	uniform	74.6176	162.6580	273.1802	398.4099	532.6899	671.3248
	linear	155.0859	334.9406	559.4693	816.5263	1101.5178	1417.3660
	nonlinear	162.5833	350.7718	585.2726	853.1769	1149.2782	1475.2611

Table 12. Critical buckling temperature ΔT_{cr} of type-I FGM rectangular thin plate with different initial temperature T_0 ($a/h = 100$, $a/b = 2$, $n = 2$).

B.C.	T.F.	$T_0 = 300$	$T_0 = 350$	$T_0 = 400$	$T_0 = 450$	$T_0 = 500$	$T_0 = 550$
CSCS	uniform	30.0846	29.1293	28.2271	27.3736	26.5646	25.7966
	linear	62.9589	61.0372	59.1907	57.4131	55.6986	54.0411
	nonlinear	66.0438	64.0307	62.0950	60.2304	58.4306	56.6896
CSCC	uniform	45.1642	43.7545	42.4210	41.1575	39.9584	38.8184
	linear	94.2791	91.4769	88.7779	86.1741	83.6574	81.2201
	nonlinear	98.8767	95.9427	93.1148	90.3846	87.7440	85.1846
CCCC	uniform	74.6176	72.3631	70.2244	68.1925	66.259	64.4162
	linear	155.0859	150.7014	146.4609	142.3542	138.3707	134.4997
	nonlinear	162.5833	157.9968	153.5573	149.2545	145.0775	141.0154

In addition, the critical temperatures are also plotted in Figures 3–6 for different thickness–length ratios h/a, power law indexes n, length–width ratios a/b and initial temperatures T_0 for type-I FGM plate. Figure 3 shows the relation between ΔT_{cr} and h/a for type-I FGM plate. The critical buckling temperature ΔT_{cr} increases as h/a increases since the thicker plates have larger bending rigidities than the thinner ones. One can also see that the critical buckling temperature of rectangular CCCC plate is the highest, whereas that of the CSCS plate is the lowest; this is because the CCCC plate has the highest bending rigidity compared with the other two cases. Furthermore, the uniform temperature field influences ΔT_{cr} more remarkably than the other two temperature fields.

Figure 4 demonstrates that ΔT_{cr} decreases as n decreases. It can be concluded from Equation (16) that the volume fraction of metal increases as n increases, and metallic materials have a lower critical buckling temperature than ceramic materials; this is because the thermal expansion coefficient α of ceramic materials is less than that of metallic materials.

Figure 5 shows the relation between ΔT_{cr} and a/b for different n. It is observed that, with a/b increasing, ΔT_{cr} increases gradually whatever n is; this indicates that the longer plates have a higher critical buckling temperature for different n. Homogeneous isotropic ceramic plate has the highest ΔT_{cr} and metallic plate has the lowest, and the volume fraction of the metal component increases as n increases.

Figure 6 indicates that ΔT_{cr} of type-I FGM plate decreases almost linearly as T_0 increases. For temperature-independent material, the ΔT_{cr} stays at a constant value, thus T_{cr} has the same increment as that of T_0. However, for type-I FGM plate, which is made from temperature-dependent materials,

ΔT_{cr} decreases almost linearly as T_0 increases, and T_{cr} increases almost linearly, but the increment of T_{cr} is less than that of T_0.

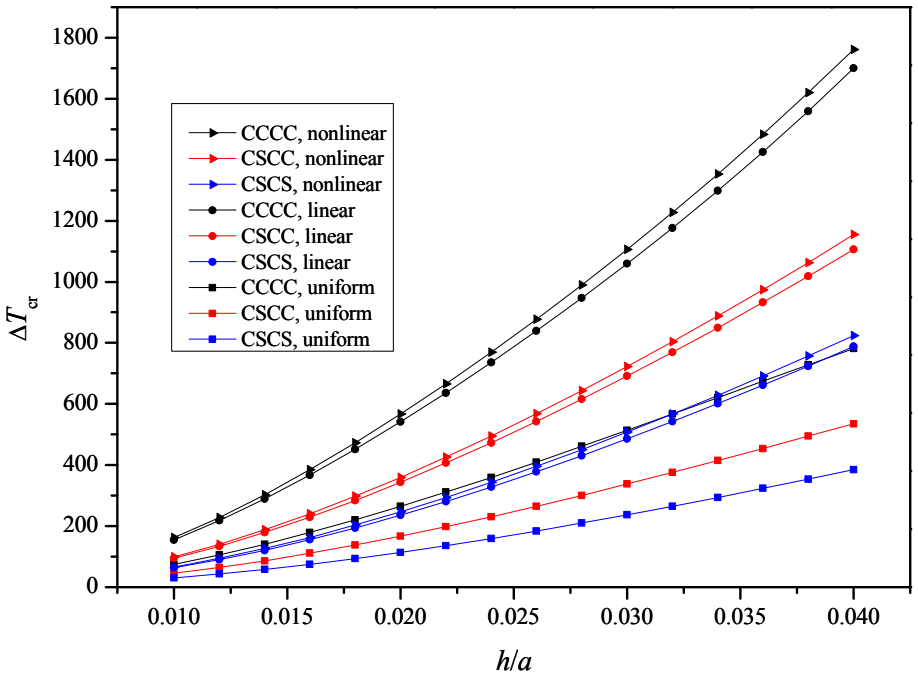

Figure 3. The relation between the critical buckling temperature ΔT_{cr} and the length–thickness ratio h/a of type-I FGM rectangular thin plate ($a/b = 2$, $n = 2$, $T_0 = 300$ K).

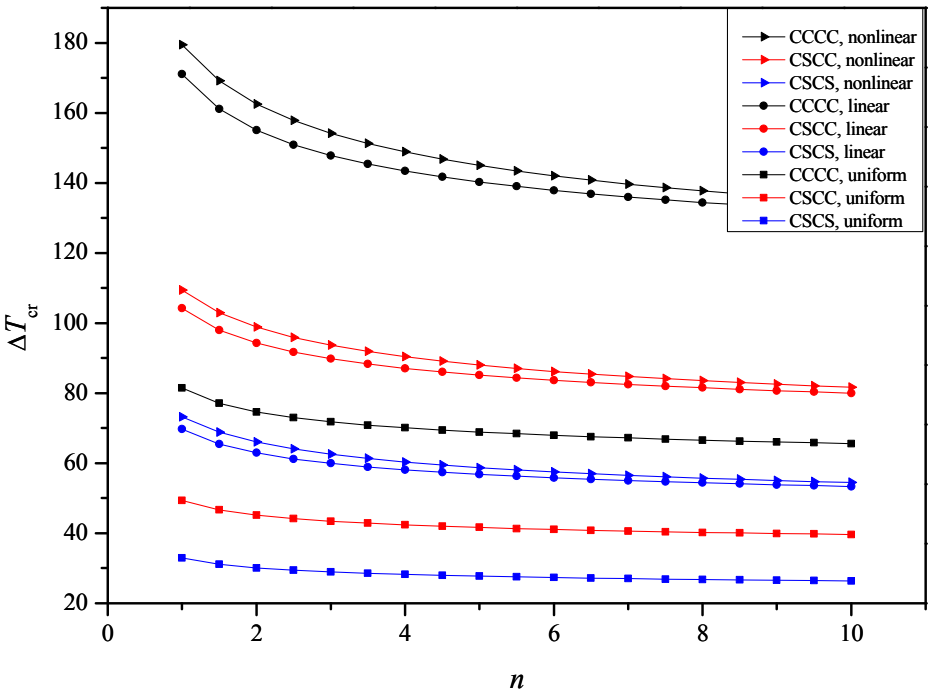

Figure 4. The relation between the critical buckling temperature ΔT_{cr} and power law index n of type-I FGM rectangular thin plate ($a/h = 100$, $a/b = 2$, $T_0 = 300$ K).

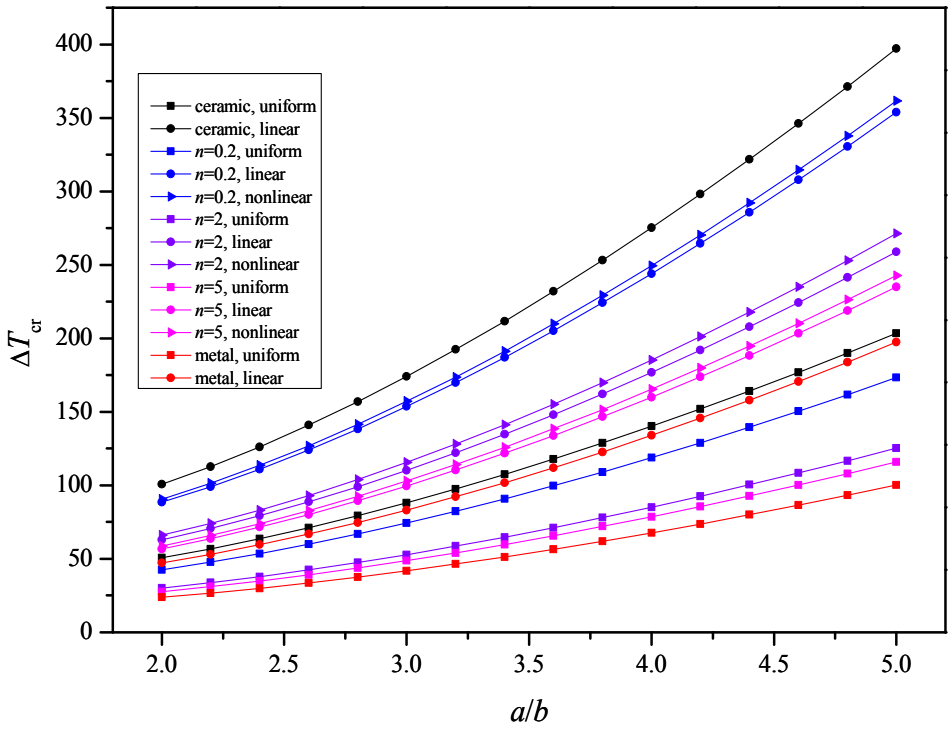

Figure 5. The relation between the critical buckling temperature ΔT_{cr} and the length–width ratio a/b of type-I FGM, ceramic and metal rectangular thin plate (a/h = 100, n = 2, T_0 = 300 K).

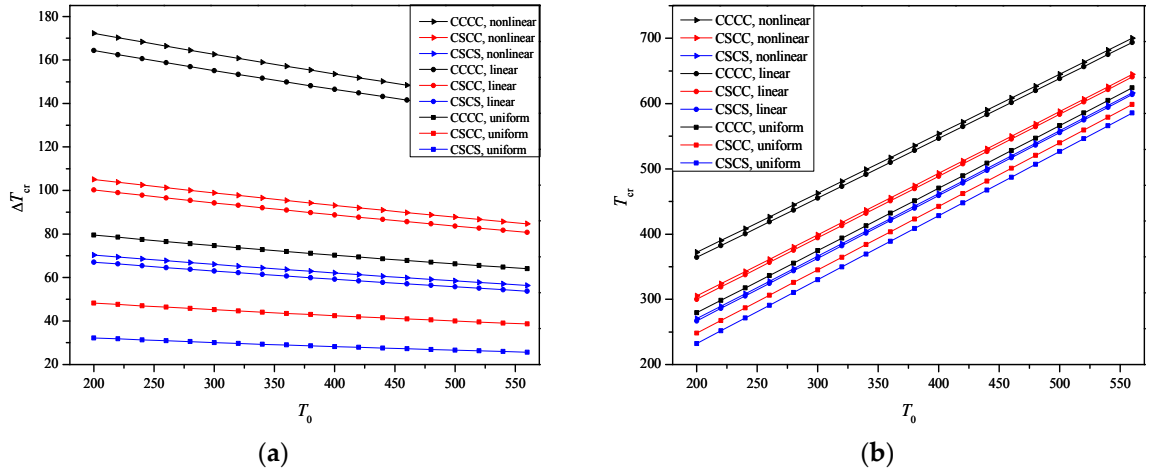

Figure 6. (**a**) The relation between ΔT_{cr} and the initial temperature T_0 of type-I FGM rectangular thin plate (a/h = 100, a/b = 2, n = 2); (**b**) The relation between T_{cr} and the initial temperature T_0 of type-I FGM rectangular thin plate (a/h = 100, a/b = 2, n = 2).

5. Conclusions

In this study, the closed form analytical solutions were obtained via the separation-of-variable method to determine the thermal buckling of FGM thin plates with simply supported, clamped and guided edges. A novel method to find the critical buckling temperature was given; the explicit expressions of the critical buckling temperature were presented for three special cases.

Two types of FGM thin plates and uniform, linear and nonlinear temperature fields were taken into account in this work. The present results coincide well with those in the literature, which illustrates the correctness of this present method. It follows that the critical buckling temperature of FGM thin plates decreases as the length–thickness ratio and power law index increase, and increases as the

length–width ratio increases, and the initial temperature affects the critical buckling temperature of temperature-dependent materials. The uniform temperature field has the greatest influence on the critical buckling temperature, and the critical buckling temperatures become very close for both linear and nonlinear temperature fields.

Acknowledgments: The work is supported by the National Natural Science Foundation of China (11372021, 11672019).

Author Contributions: Y.X. conceived the research ideas; Z.W. derived equations, calculated and analyzed numerical results; both authors participated in the writing of this article.

Conflicts of Interest: The authors declare no conflict of interest.

Appendix A

Table A1. Coefficients of Equation (41).

A_9	$\nu_0\alpha_3\nu_3$
A_8	$\nu_0(8T_0\gamma_1+\gamma_2)$
A_7	$\nu_0\left(28{T_0}^2\gamma_1+7T_0\gamma_2+\gamma_3\right)$
A_6	$\nu_0\left(56{T_0}^3\gamma_1+21{T_0}^2\gamma_2+6T_0\gamma_3+\gamma_4\right)+\alpha_3$
A_5	$\nu_0\left(70{T_0}^4\gamma_1+35{T_0}^3\gamma_2+15{T_0}^2\gamma_3+5T_0\gamma_4+\gamma_5\right)+(5T_0\alpha_3+\alpha_2)$
A_4	$\nu_0\left(56{T_0}^5\gamma_1+35{T_0}^4\gamma_2+20{T_0}^3\gamma_3+10{T_0}^22\gamma_4+4T_0\gamma_5+\gamma_6\right)$ $+\left(10{T_0}^2\alpha_3+4T_0\alpha_2+\alpha_1\right)$
A_3	$\nu_0\left(28{T_0}^6\gamma_1+21{T_0}^5\gamma_2+15{T_0}^4\gamma_3+10{T_0}^3\gamma_4+6{T_0}^2\gamma_5+3T_0\gamma_6+\gamma_7\right)$ $+\left(10{T_0}^3\alpha_3+6{T_0}^2\alpha_2+3T_0\alpha_1+1\right)$
A_2	$\nu_0\left(8{T_0}^7\gamma_1+7{T_0}^6\gamma_2+6{T_0}^5\gamma_3+5{T_0}^4\gamma_4+4{T_0}^3\gamma_5+3{T_0}^2\gamma_6+2T_0\gamma_7+\gamma_8\right)$ $+\left(5{T_0}^4\alpha_3+4{T_0}^3\alpha_2+3{T_0}^2\alpha_1+2T_0+\alpha_{-1}\right)-\dfrac{\hat{G}_{0cr}h^2}{\alpha_0+\left(\hat{G}_{0\mathrm{cr}}h^2+12\right)}$
A_1	$\nu_0\begin{pmatrix}{T_0}^8\gamma_1+{T_0}^7\gamma_2+{T_0}^6\gamma_3+{T_0}^5\gamma_4+{T_0}^4\gamma_5\\ +{T_0}^3\gamma_6+{T_0}^2\gamma_7+T_0\gamma_8+\nu_{-1}\alpha_{-1}\end{pmatrix}$ $+\left({T_0}^5\alpha_3+{T_0}^4\alpha_2+{T_0}^3\alpha_1+{T_0}^2+T_0\alpha_{-1}\right)-\dfrac{2\hat{G}_{0\mathrm{cr}}h^2T_0}{\alpha_0\left(\hat{G}_{0\mathrm{cr}}h^2+12\right)}$
A_0	$-\dfrac{\hat{G}_{0cr}h^2T_0}{\alpha_0\left(\hat{G}_{0cr}h^2+12\right)}$

where

$$\begin{aligned}
\gamma_1 &= \alpha_3\nu_3\\
\gamma_2 &= \alpha_2\nu_3+\alpha_3\nu_2\\
\gamma_3 &= \alpha_1\nu_3+\alpha_2\nu_2+\alpha_3\nu_1\\
\gamma_4 &= \alpha_1\nu_2+\alpha_2\nu_1+\alpha_3+\nu_3\\
\gamma_5 &= \alpha_1\nu_1+\nu_3\alpha_{-1}+\nu_{-1}\alpha_3+\alpha_2+\nu_2\\
\gamma_6 &= \nu_2\alpha_{-1}+\nu_{-1}\alpha_2+\nu_1+\alpha_1\\
\gamma_7 &= \nu_{-1}\alpha_1+\nu_1\alpha_{-1}+1\\
\gamma_8 &= \alpha_{-1}+\nu_{-1}
\end{aligned} \tag{A1}$$

References

1. Koizumi, M. The concept of FGM. *Funct. Gradient Mater.* **1993**, *34*, 3–10. [CrossRef]
2. Koizumi, M. FGM activities in Japan. *Compos. Part B Eng.* **1997**, *28*, 1–4. [CrossRef]
3. Javaheri, R.; Eslami, M.R. Thermal buckling of functionally graded plates. *AIAA J.* **2002**, *40*, 162–184. [CrossRef]
4. Shariat, B.S.; Eslami, M.R. Thermal buckling of imperfect functionally graded plates. *Int. J. Solids Struct.* **2006**, *43*, 4082–4096. [CrossRef]
5. Kiani, Y.; Bagherizadeh, E.; Eslami, M.R. Thermal buckling of clamped thin rectangular FGM plates resting on Pasternak elastic foundation (three approximate analytical solutions). *J. Appl. Math. Mech.* **2011**, *91*, 581–593. [CrossRef]
6. Chu, F.; He, J.; Wang, L.; Zhong, Z. Buckling analysis of functionally graded thin plate with in-plane material inhomogeneity. *Eng. Anal. Bound. Elem.* **2016**, *65*, 112–125. [CrossRef]
7. Wu, L. Thermal buckling of a simply supported moderately thick rectangular FGM plate. *Compos. Struct.* **2004**, *64*, 211–218. [CrossRef]
8. Bouazza, M.; Tounsi, A.; Adda-Bedia, E.A.; Megueni, A. Thermoelastic stability analysis of functionally graded plates: An analytical approach. *Comput. Mater. Sci.* **2010**, *49*, 865–870. [CrossRef]
9. Shariat, B.S.; Eslami, M.R. Effect of initial imperfections on thermal buckling of functionally graded plates. *J. Therm. Stress.* **2005**, *28*, 1183–1198. [CrossRef]
10. Lee, Y.H.; Bae, S.I.; Kim, J.H. Thermal buckling behavior of functionally graded plates based on neutral surface. *Compos. Struct.* **2016**, *137*, 208–214. [CrossRef]
11. Park, J.S.; Kim, J.H. Thermal postbuckling and vibration analyses of functionally graded plates. *J. Sound Vib.* **2006**, *289*, 77–93. [CrossRef]
12. Cong, P.H.; Duc, N.D. Thermal stability analysis of eccentrically stiffened sigmoid-FGM plate with metal–ceramic–metal layers based on FSDT. *Cogent Eng.* **2016**, *3*. [CrossRef]
13. Javaheri, R.; Eslami, M.R. Thermal buckling of functionally graded plates based on higher order theory. *J. Therm. Stress.* **2002**, *25*, 603–625. [CrossRef]
14. Najafizadeh, M.M.; Heydari, H.R. Thermal buckling of functionally graded circular plates based on higher order shear deformation plate theory. *Eur. J. Mech. A/Solids* **2004**, *23*, 1085–1100. [CrossRef]
15. Matsunaga, H. Thermal buckling of functionally graded plates according to a 2D higher-order deformation theory. *Compos. Struct.* **2009**, *90*, 76–86. [CrossRef]
16. Zenkour, A.M.; Mashat, D.S. Thermal buckling analysis of ceramic-metal functionally graded plates. *Nat. Sci.* **2010**, *2*, 968–978. [CrossRef]
17. Na, K.S.; Kim, J.H. Three-dimensional thermal buckling analysis of functionally graded materials. *Compos. Part B Eng.* **2004**, *35*, 429–437. [CrossRef]
18. Na, K.S.; Kim, J.H. Three-dimensional thermomechanical buckling analysis for functionally graded composite plates. *Compos. Struct.* **2006**, *73*, 413–422. [CrossRef]
19. Malekzadeh, P. Three-dimensional thermal buckling analysis of functionally graded arbitrary straight-sided quadrilateral plates using differential quadrature method. *Compos. Struct.* **2011**, *93*, 1246–1254. [CrossRef]
20. Asemi, K.; Shariyat, M.; Salehi, M.; Ashrafi, H. A full compatible three-dimensional elasticity element for buckling analysis of FGM rectangular plates subjected to various combinations of biaxial normal and shear loads. *Finite Elem. Anal. Des.* **2013**, *74*, 9–21. [CrossRef]
21. Swaminathan, K.; Sangeetha, D.M. Thermal analysis of FGM plates—A critical review of various modeling techniques and solution methods. *Compos. Struct.* **2017**, *160*, 43–60. [CrossRef]
22. Xu, T.F.; Xing, Y.F. Closed-form solutions for free vibration of rectangular FGM thin plates resting on elastic foundation. *Acta Mech. Sin.* **2016**, *32*, 1088–1103. [CrossRef]
23. Bouhadra, A.; Benyoucef, S.; Tounsi, A.; Bernard, F.; Bouiadjra, R.B.; Sid Ahmed Houari, M. Thermal buckling response of functionally graded plates with clamped boundary conditions. *J. Therm. Stress.* **2015**, *38*, 630–650. [CrossRef]
24. Thornton, E.A. Thermal buckling of plates and shells. *Appl. Mech. Rev.* **1993**, *46*, 485–506. [CrossRef]
25. Xing, Y.F.; Liu, B. New exact solutions for free vibrations of rectangular thin plates by symplectic dual method. *Acta Mech. Sin.* **2009**, *25*, 265–270. [CrossRef]

26. Xing, Y.F.; Liu, B. New exact solutions for free vibrations of thin orthotropic rectangular plates. *Compos. Struct.* **2009**, *104*, 187–195. [CrossRef]
27. Xing, Y.F.; Xu, T.F. Solution methods of exact solutions for free vibration of rectangular orthotropic thin plates with classical boundary conditions. *Compos. Struct.* **2013**, *104*, 187–195. [CrossRef]